Algorithms for point target detection in hyperspectral imagery

C. E. Caefer[*a], S.R. Rotman[*b], J. Silverman[*a], and P.W. Yip[*a]
[a]Air Force Research Laboratory, Hanscom AFB; [b]Ben-Gurion Univ. of the Negev

ABSTRACT

Two techniques for detecting point targets in hyperspectral imagery are described. The first technique is based on the principal component analysis of hyperspectral data. We combine the information of the first two principal component analysis images; the result is a single image display "summary" of the data cube. The summary frame is used to define image segments. The statistics, means and variances, of each segment for the principal component images is calculated and a covariance matrix is constructed. The local pixel statistics and the segment statistics are then used to evaluate the extent to which each pixel differs from its surroundings. Point target pixels will have abnormally high values. The second technique operates on each band of the hypercube. A local anti-median of each pixel is taken and is weighted by the standard deviation of the local neighborhood. The results of each band are then combined. Results will be shown for visible, SWIR, and MWIR hyperspectral imagery.

Keywords: hyperspectral data, point target detection

1. INTRODUCTION

Many sophisticated techniques have been developed to detect point targets in natural backgrounds. The evolution of detection and tracking algorithms used in Infrared Search and Track (IRST) systems, from single frame detection and subsequent tracking to advanced multi-frame signal processing algorithms, has been described by Chan[1]. Typically, spatial filters operate on individual frames producing candidate "hits" followed by a tracking stage[2]. In our earlier work we developed spatial temporal filters for IRST.[3-5] With the advent of multi- and hyperspectral cameras, we believe the spectral domain will become a necessary component of many point target detection algorithms. In this paper we describe two spatial filters for point target detection in hyperspectral imagery, the Principal Component Analysis (PCA) algorithm and the Weighted Anti-Median (WAM) algorithm. Next we present our technique for generating Receiver Operating Characteristic (ROC) curves, describe our data sets, and finally present results and conclusions.

2. PRINCIPAL COMPONENT ANALYSIS ALGORITHM

In designing this algorithm, we assumed that, although principal components are statistically independent from each other over the entire image, there are segments where correlations between principal components still remain. The data can be modeled as quasi-stationary adjacent segments. Most pixels within a neighborhood belong to the same segment; only a few pixels are located on the boundaries between segments.

The first step in the PCA Algorithm is to obtain the first two principal component images of the data cube. Fig 1 shows one frame taken from a MWIR data cube with 12 embedded targets. We created these embedded targets by simply transplanting a bright pixel to other locations in the hypercube. Figs. 2a and 2b are the first and second principal component images of the MWIR data. We combine the information from the first two principal component images, using an algorithm described by Silverman[6] et al., and the result is a single segmented image as shown in Fig. 2c. Our inherently non-stationary hyperspectral data cube is now represented by quasi-stationary segments. Next, we evaluate the means and variances of each segment for the two principal component images and construct the covariance matrix of each segment.

*charlene.caefer@hanscom.af.mil; phone 781 377-2875; fax 781 377-4814; Sensors Directorate, Air Force Research Laboratory, AFRL/SNHI, 80 Scott Rd., Hanscom AFB, MA USA 01731; **srotman@ee.bgu.ac.il; phone +972-8-6413539; fax +972-8-6472949; Ben-Gurion University, Dept. of Elec. Eng., P.O. Box 653 Beer-Sheva, 84105 ISRAEL.

Imaging Spectrometry VIII, Sylvia S. Shen, Editor, Proceedings of SPIE Vol. 4816
(2002) © 2002 SPIE · 0277-786X/2002/$15.00

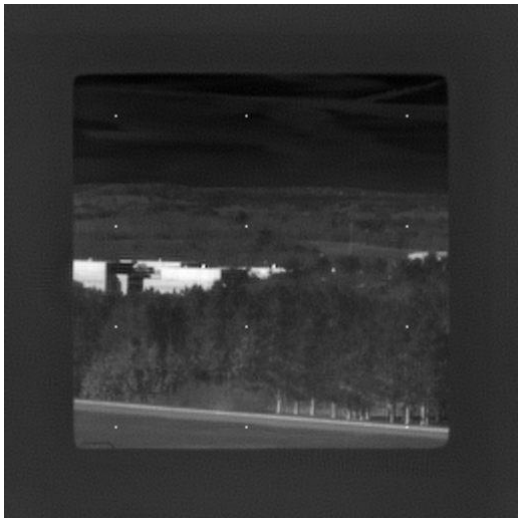

Fig. 1. MWIR image with 12 embedded targets

Fig. 2d shows the final result of our algorithm as an image whose pixel values **S** represent the extent to which it differs from to its surroundings. The statistics of the pixel's neighborhood and the statistics of its segment are used to weight the result. Each pixel is assigned a value using the standard statistic for a two-dimensional gaussian[7] as described in the following equations.

$$\mathbf{S = (x - m)^T \Lambda^{-1}_{SEG} (x - m)} \tag{1}$$

$$\mathbf{x} = (x_1, x_2) \tag{2}$$

$$\mathbf{m} = (m_1, m_2) \tag{3}$$

$$\Lambda_{SEG} = \begin{bmatrix} \sigma^2_{x_1} & \sigma^2_{x_1,x_2} \\ \sigma^2_{x_2,x_1} & \sigma^2_{x_2} \end{bmatrix} \quad \Lambda^{-1}_{SEG} = \frac{1}{\sigma^2_{x_1}\sigma^2_{x_2} - \sigma^2_{x_1,x_2}\sigma^2_{x_2,x_1}} \begin{bmatrix} \sigma^2_{x_2} & \sigma^2_{x_2,x_1} \\ \sigma^2_{x_1,x_2} & \sigma^2_{x_1} \end{bmatrix} \tag{4}$$

The vector **x** has two values (x_1, x_2), x_1 is the pixel value from the first principal component image and x_2 is the pixel value from the second principal component. Similarly, the vector **m** has two values (m_1, m_2), one for each of the principal component images. The vector **m** is the local median; the median is generated using its 8 closest neighbors. Therefore, (**x-m**) is the anti-median. The values of the inverse covariance matrix $\mathbf{\Lambda_x^{-1}}$ are taken from the "segment" to which the largest number of neighborhood pixels belong. At least five of the eight neighboring pixels must belong to the same segment for the pixel to be evaluated. At present, pixels that do not meet this criterion are not evaluated. Further research is needed to estimate the statistics of these pixels, most of which fall on the borders of segments.

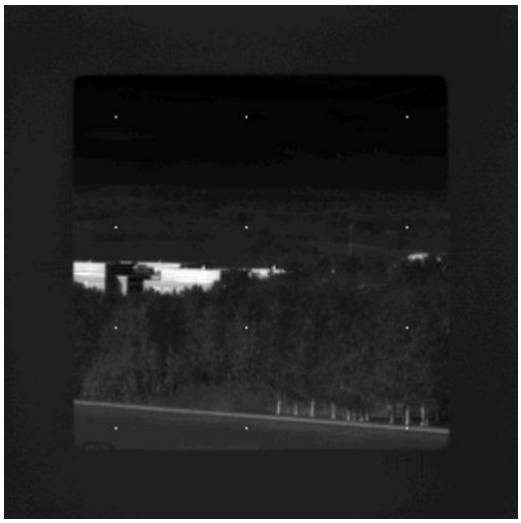

Fig. 2a. First principal component image

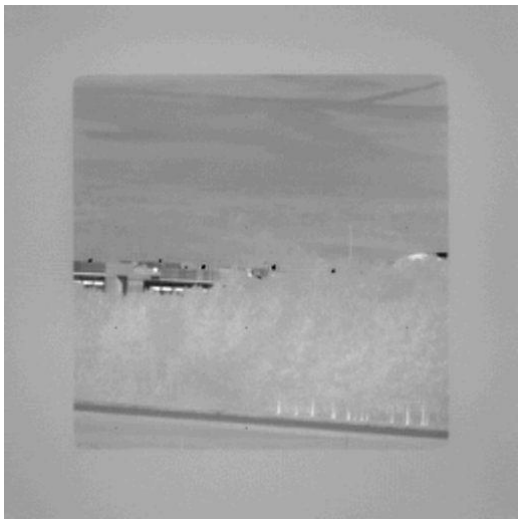

Fig. 2b. Second principal component image

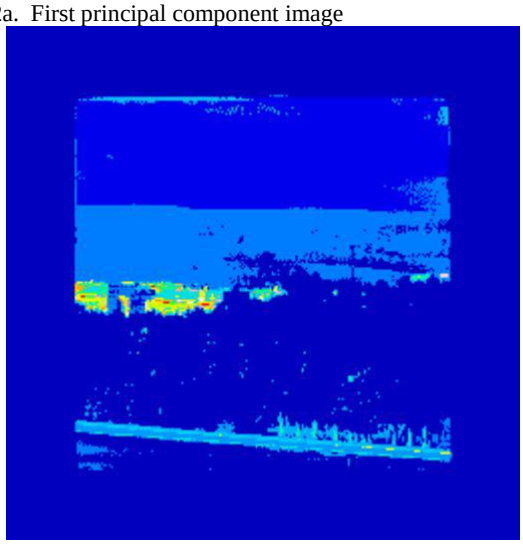

Fig. 2c. Segmented image

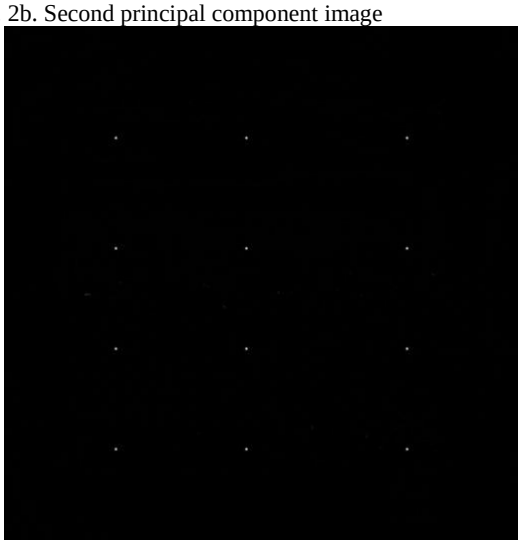

Fig. 2d. Principal component analysis algorithm result

3. WEIGHTED ANTI-MEDIAN ALGORITHM

The weighted anti-median algorithm processes the entire data cube band by band, in contrast to our previous algorithm which was run using the first two principal components. The first step of the weighted anti-median algorithm is to calculate the local statistics of each pixel for each band. The median and standard deviation of each pixel is generated using the 8 closest neighbors of the pixel. Each pixel in the image is given a value according to the following equation:

$$D = (x_i - m_i)/ \sigma_i \qquad (5)$$

The value x_i is the value of the pixel in band i, m_i is the local median and σ_i is the local standard deviation. The results of applying Eq. (5) to the hyperspectral data illustrated in Fig. 1 are shown in Fig. 3. Fig. 3a shows a single band result using just the numerator of Eq. (5) and Fig. 3b shows a single band result weighted by the standard deviation. The division by the standard deviation definitely enhances the targets relative to the background. Note the difficulty the algorithm has in detecting the lower right target. The target is on the road and the road pixels are not very different in magnitude from the embedded pixel.

Next we combine the results of each band, which makes a comparison between the results of the two algorithms possible. Paglieroni and Perkins[8] has suggested thresholding each image, band by band, and designating a pixel a target if it is above the threshold in any band. In this paper, we will present two linear weighting combinations of the band results. The first is a uniform weighting of all the bands, i.e., a sum. For the second method, we construct a quasi-matched filter. We use as weighting coefficients the values for each band given by the first eigenchroma of the principal components of the entire data cube. If the cube is composed of a unique signal (at different levels for each pixel but with the same spectral shape) plus a low level of spectrally and spatially uncorrelated noise, the first eigenchroma would be proportional to the signal. This would be appropriate for a matched filter. We recognize that these assumptions are violated in most hyperspectral images; thus, this weighting algorithm should be considered as a rough approximation of the optimum filter.

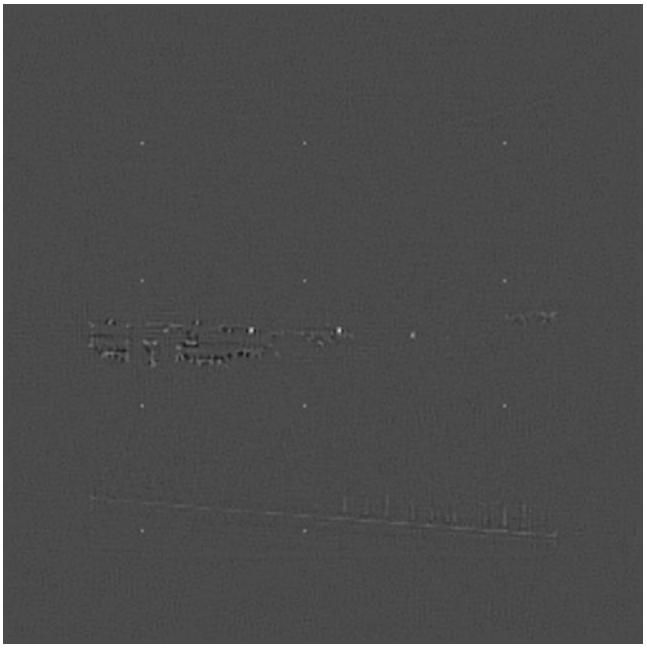

Fig. 3a. Single frame anti-median algorithm

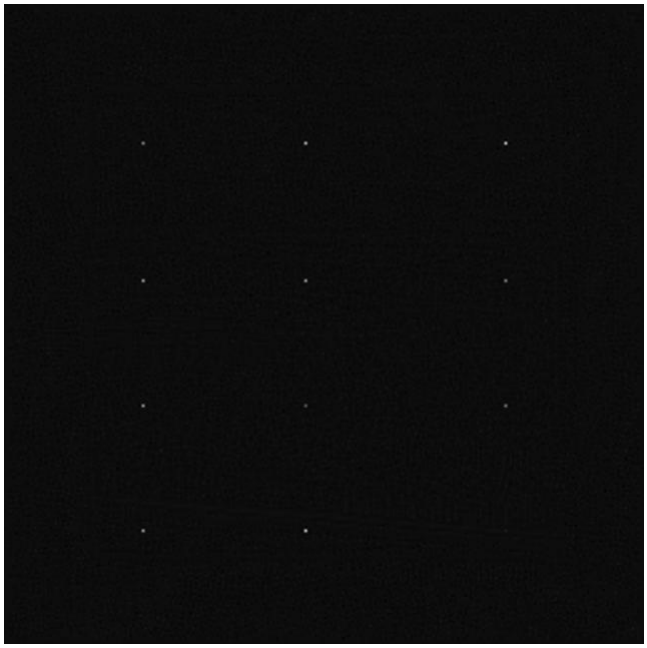

Fig. 3a. Single frame weighted anti-median algorithm

4. ROC CURVE GENERATION

To evaluate the algorithms over a wide spectrum of targets and target locations, we embedded point targets in our hyperspectral data sets. We embedded targets as follows; we find one of the brightest pixels in the first principal component image and designate it as target pixel **y**. Then we transplant a fraction f of this vector to the background pixel **b.** Thus, the new pixel **z** replaces the background pixel **b**:

$$\mathbf{z} = f\,\mathbf{y} + (1.0 - f)\mathbf{b} \qquad (6)$$

This process is done for each band in the cube. In the interest of visual clarity, f equals 1.0 in Figures 1-3:, i.e., the target pixel replaces the background pixel. The values of f actually used to evaluate the algorithms ranged from 0.01 (1%) to 0.10 (10%) in steps of 0.01 (1%).

We compare the efficacy of the two algorithms for particular target strength by using classical ROC (Receiver Operating Characteristic) curves. The technique is as follows (as described in Bar-Tal and Rotman as given in Ref. 3): First we operate on the raw data, i.e., without any embedded targets. We evaluate for each pixel the algorithm being tested using Eq. (1) for the PCA algorithm and Eq. (5) for the WAM algorithm. The results are summarized in what we call a no-target histogram. Next we embed targets into every pixel location and evaluate the algorithm under study. This is done independently for each pixel location (rather than simultaneously) so that surrounding pixels are not changed prior to the

algorithm evaluation. The results are placed in a target histogram. For each histogram (no-target and target) the following steps are taken. Each histogram is normalized and a cumulative probability histogram is calculated. Subsequently one minus the value of the cumulative probability histogram is computed giving us the inverse cumulative probability distributions for both the no-target and target cases. The x-axis of these distributions are the values of the pixels from Eq. (1) or Eq. (5); the y-axis is the value of the probability of false alarm and the probability of detection taken from the no-target and target-present inverse cumulative probability distribution, respectively, for that pixel value. For each threshold in the histograms we obtain a pair of values corresponding to the probability of detection and probability of false alarm; and using these pairs we generate our ROC curve.

To summarize, the steps to evaluate the ROC curves are as follows:

1. Run the algorithm on the data cube with an embedded target in every pixel location.
   (The target is not in all the positions simultaneously; rather the result is obtained sequentially.)
2. Generate a histogram of the algorithm result for embedded targets.
3. Generate a cumulative histogram of the algorithm result for embedded targets.
   (Normalize to number of pixels evaluated.)
4. Generate an inverse cumulative probability distribution (1.0-cumulative histogram), using result from step 3
   (These are the Probability of Detection (P_D) values.)
5. Run the algorithm on the original data cube in which no targets have been implanted.
6. Generate a histogram of the algorithm result for no targets.
   (Use same scale as step 2.)
7. Generate a cumulative histogram of the algorithm result for no targets.
   (Normalize to number of pixels evaluated)
8. Generate an inverse cumulative probability distribution (1.0-cumulative histogram), using result from step 7
   (These are the Probability of False Alarm (P_{FA}) values.)
9. Plot the Probability of Detection values (step 4) versus Probability of False Alarm values (step 8).

Every point on a ROC curve represents a possible position of the threshold for determining the presence of a target. To generate a single metric for quantifying the ability of a particular algorithm to detect the target and reject false alarms, we evaluate the area under the ROC curve minus 0.5. The value of 0.5 represents the area under the ROC curve for the case where the target is not contributing to the pixel values, i.e. the target is completely indistinguishable from the background. In such a case, for all thresholds, P_{FA} would equal P_D. Hence, the value of this metric (the area under the ROC curve minus 0.5) measures the ability of an algorithm to discriminate target from background.

5. DATA DESCRIPTION

The algorithms under study assume the data can be modeled as quasi-stationary segments that are located adjacent to each other. We assume that for most pixels the immediate surroundings of the pixel will belong to a stationary background. Only a few pixels are located on the boundaries between segments. Much natural imagery in the visible and the infrared can be described in this manner. The algorithms we developed are not band specific; we have found these techniques give reasonable results over many scenes and wavelength bands. We will restrict our sample results to the following three spectral ranges: visible, MWIR, and SWIR. The visible hyperspectral data was taken with an AFRL/Solid State Scientific Corporation chromotomographic hyperspectral imaging sensor (CTHIS). The camera design, performance and signal processing characteristics have been described previously[9]. The MWIR hyperspectral image was also taken with an in-house imaging spectrometer. The imager used is the next generation of the prototype described in earlier work.[10] Finally the SWIR data is extracted from a HYDICE image provided by Spectral Information Technology Application Center (SITAC). HYDICE is a pushbroom imaging spectrometer with 210 spectral bands, which cover the full 0.4 to 2.5 μm spectral range. The array is a 320x210 element InSb array[11]. The size of the extracted image is 187 by 259 pixels and was taken over the CART/ARM Site, Lamont, OK, in early evening at 11,400'.

6. RESULTS

We next turn to analyzing the results of these techniques using data from three different bands. The results will be shown pictorially and numerically. We will first analyze the MWIR image presented earlier in Fig. 1. Fig. 4a shows the result of running the principal component algorithm on the MWIR data set without any embedded targets. Fig. 4b and Fig. 4c show the result of the principal component analysis algorithm run on data sets with embedded targets of strengths 2% and 8%, respectively. Fig. 4d, 4e, 4f are the analogous results for the weighted anti-median algorithm.

In Fig. 4 (and as well later in Figures 7 and 10), each image is scaled linearly such that the lowest value is displayed as 0 and the highest value is displayed as 255. Thus, no comparison can be made from image to image simply on the basis of the brightness of a particular pixel. Rather, the significance of these pictures is in the relative brightness of the pixels within each image: the brightness in the "no target" and "embedded target" images is related to the probability of false alarm and detection, respectively.

The images with no targets effectively represent the deviations of normal pixels from their surroundings. In Eq. (1), if a pixel's vector equals the median vector, the value of S equals 0. There are many pixels for which this is true, and hence Fig. 4a have many dark pixels. In Fig. 4d, derived from Eq. (5), the lowest pixel D will be caused by that pixel which is most negative relative to its median. Assuming a normal distribution for the values of D in Fig. 4d, we would expect very few pixels with this value and many pixels with value 0 (displayed as 128 out of 255). This explains the relative paucity of pixels with the lowest value.

The insertion of higher fractions of the target causes a stronger differentiation between various segments of the image. As the fraction rises, the change in the pixel value is greater than the natural noise present in the image. In Figs. 4b-4c the addition of the target fraction causes all pixel values to change except for the area where target pixel was selected, i.e., the building. Thus, in Fig. 4c and 4d, the buildings (and the road which is similar in spectral values) remain dark. The sky, which is most dissimilar to the building, is the one most greatly effected by the presence of the target fraction. Similarly, in Figs. 4d to 4f, the values D rise with the target fraction. The field stop surrounding the image is one of the most uniform and darkest regions in the picture and hence is greatly changed between Figs. 4d to 4f. The building becomes blacker since it maintains a value close to 0.

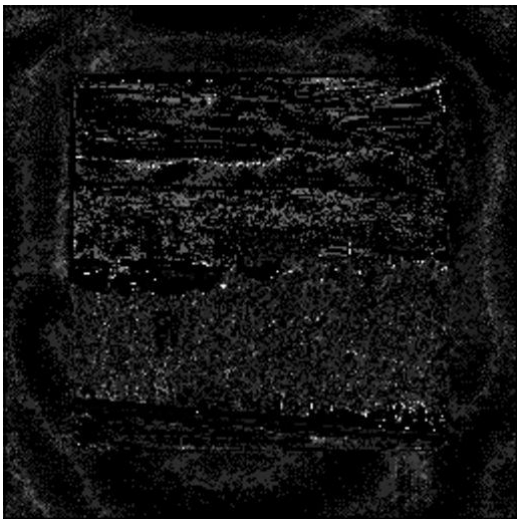

Fig. 4a. PCA algorithm result - no target.

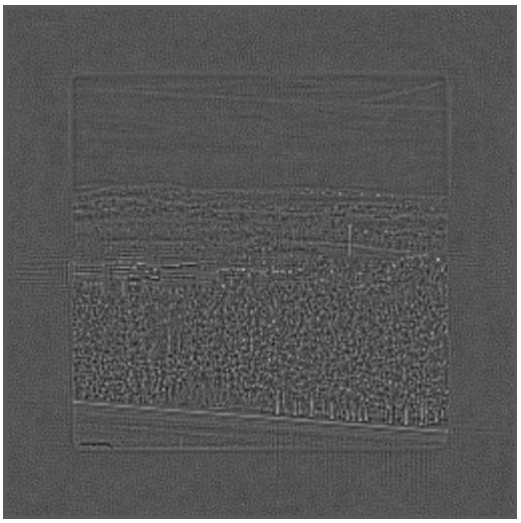

Fig. 4d. Eigenchroma – WAM algorithm result - no target.

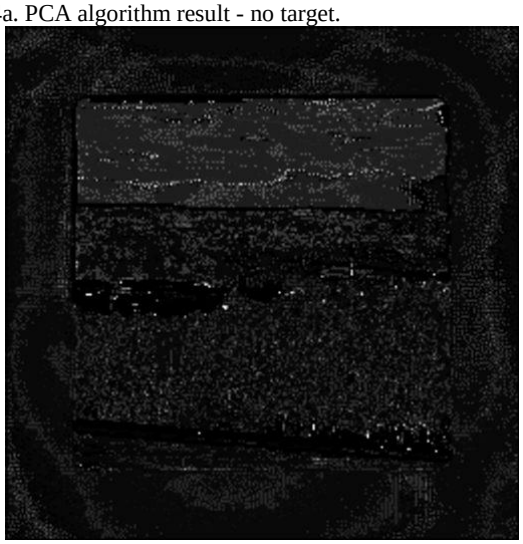

Fig. 4b. PCA algorithm result - 2% target.

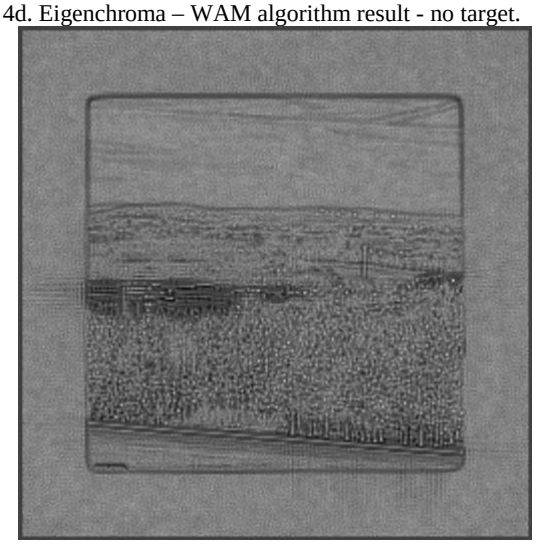

Fig. 4e. Eigenchroma -WAM algorithm result - 2% target.

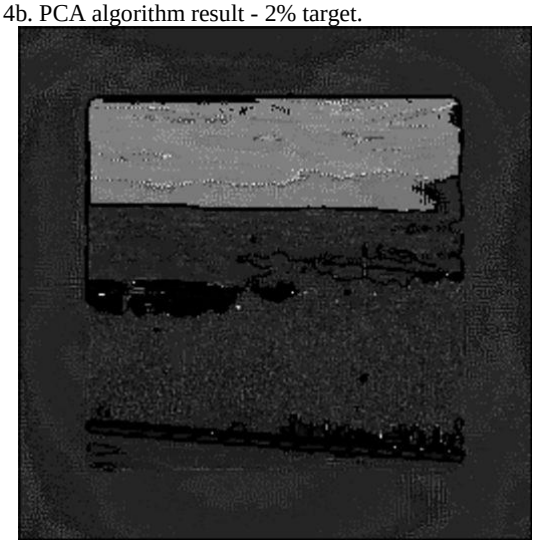

Fig. 4c. PCA algorithm result - 8% target.

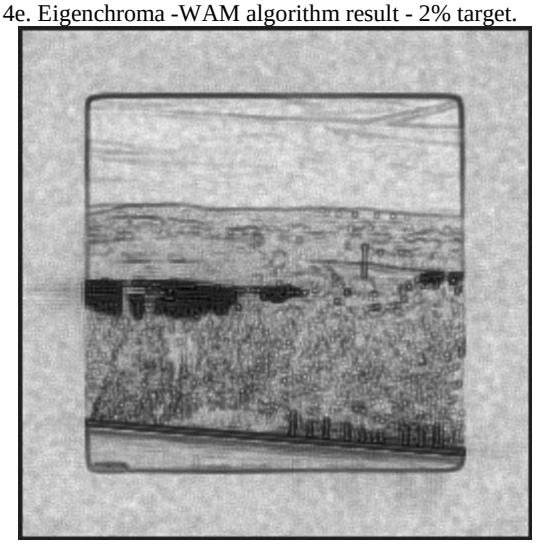

Fig. 4f. Eigenchroma – WAM algorithm result - 8% target.

The target pixel is a transplanted building pixel; for this reason both algorithms have trouble with pixels in the building. Both algorithms are in essence anomaly detectors and in the building segment, this pixel is not anomalous. Table 1 summarizes the results for the algorithms when run on targets ranging from 1% to 10 %. The values in the table are the areas under the ROC curve minus 0.5.

Table 1. MWIR Results.

Percent Target	PCA	Sum WAM	Eigenchroma WAM	Sum AM	Eigenchroma AM
1	0.205	0.352	0.395	0.130	0.355
2	0.231	0.443	0.461	0.244	0.436
3	0.331	0.470	0.479	0.331	0.464
4	0.433	0.481	0.486	0.391	0.475
5	0.461	0.486	0.489	0.429	0.481
6	0.487	0.488	0.491	0.453	0.484
7	0.494	0.490	0.492	0.467	0.486
8	0.497	0.491	0.493	0.475	0.488
9	0.498	0.492	0.494	0.481	0.489
10	0.498	0.493	0.494	0.484	0.490

The last two columns of the table represent the results of the anti-median before it is weighted by the standard deviation. These columns show the necessity of weighting a pixel by the degree of noise in the surroundings. When comparing the columns labeled Sum-Weighted Anti-Median and Eigenchroma - Weighted Anti-Median, the Eigenchroma column gives better results. Finally, the results from the principal component analysis algorithm give lower values than either of the weighted anti-median results. The improvement of the anti-median filter over the principal component analysis is not due simply to the fact that the anti-median filter is only affected by “bright” targets while the principal component method is affected by “unusual” (bright or dark) targets. We have found that the superiority of the WAM method is maintained even if the absolute value of the difference is used instead of the simple difference as in Eq. (5). It appears that there is an inherent superiority to processing each band of the hyperspectral cube and summing the results over the bands as opposed to using one or two summations of the data, as is the case in the PCA algorithm. This points to the benefits of using hyperspectral data in point target detection over broadband imagery.

Fig. 5 is the summary ROC curve generated for the 2% embedded target. Note the superior performance of the weighted anti-median techniques at the low false alarm regions.

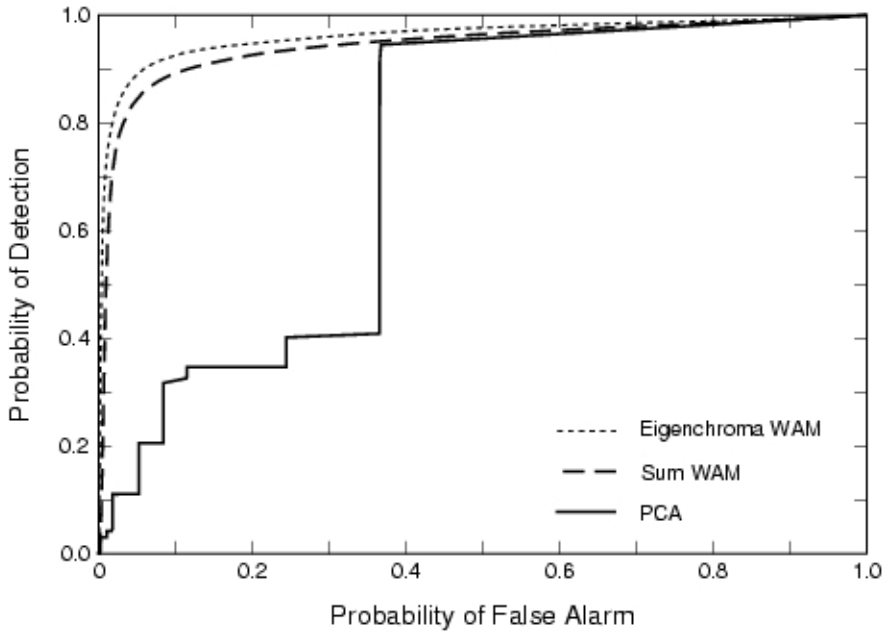

Fig. 5. ROC curves for 2 % target embedded in MWIR image.

Next we will look at our visible hyperspectral data example. Fig.6a shows a representative image from the data cube.

Fig. 6. Representative frame from visible hyperspectral datacube. Embedded pixel extracted from equipment in center of image.

Fig. 7 is a summary of the results for the visible data. It is arranged in the same way as Fig. 4, but the embedded targets have strengths of 3% and 8%.

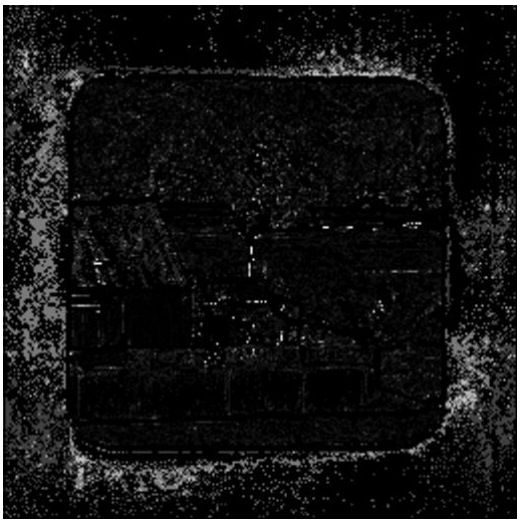

Fig. 7a. PCA algorithm result - no target.

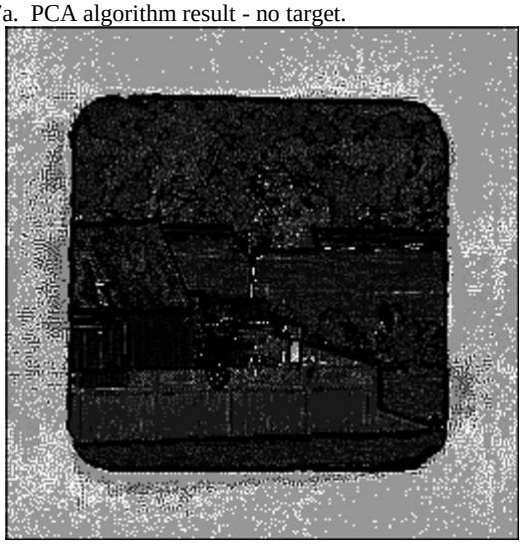

Fig. 7b. PCA algorithm result - 3% target.

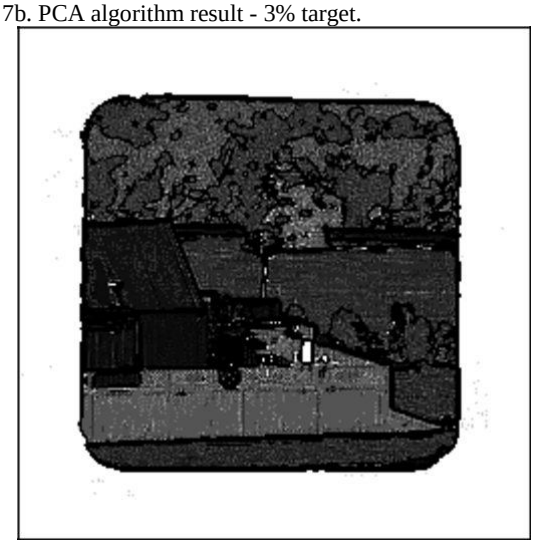

Fig. 7c. PCA algorithm result - 8% target.

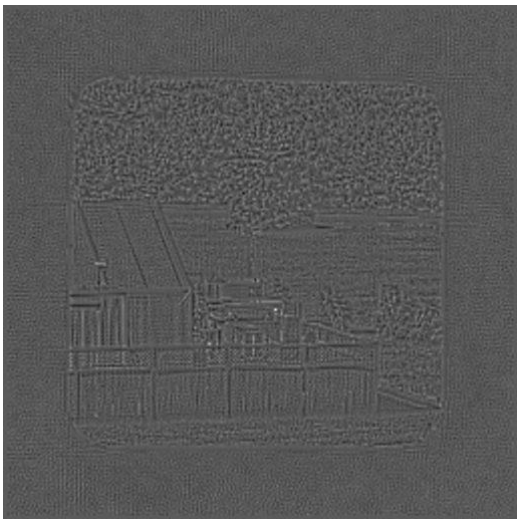

Fig. 7d. Eigenchroma – WAM algorithm result - no target.

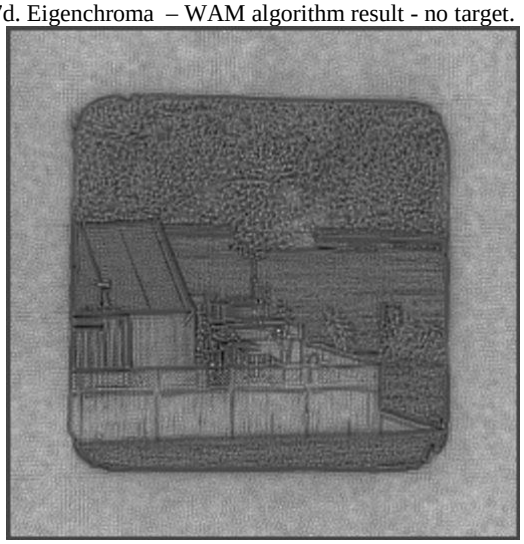

Fig. 7e. Eigenchroma – WAM algorithm result - 3% target.

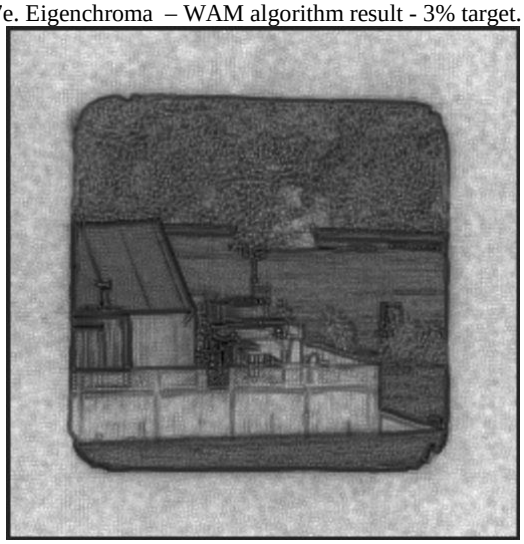

Fig. 7f. Eigenchroma – WAM result - 8% target.

Table 2 summarizes the results for the algorithms when run on targets ranging from 1% to 10 %. The values in the table are areas under the ROC curve minus 0.5. Once again the weighted anti-median algorithm gives the best results. One notable difference from the MWIR case is that the Eigenchroma weighted sum gives a better result than the sum in only the 1% case. Fig. 8. shows the ROC curves for a 3% target. This result shows a slight improvement of the sum weighted anti-median over the Eigenchroma sum weighted anti-median algorithm. The first Eigenchroma is not the optimum weighting of the bands. The first eigenchroma would have been the optimum weighting if: 1. the target signal were proportional to a single endmember and 2. if the noise in these bands after passing through the anti-median filter were uncorrelated from band to band. We are engaging in additional research to theoretically model the optimum weighting of infrared images after median filtering even if these assumptions are not fulfilled. The principal component analysis algorithm is not performing as well as the weighted anti-median algorithm.

Table 2. Visible Results

Percent Target	PCA	Sum WAM	Eigenchroma WAM
1	0.182	0.276	0.285
2	0.304	0.386	0.375
3	0.372	0.435	0.420
4	0.403	0.461	0.448
5	0.429	0.475	0.465
6	0.449	0.483	0.476
7	0.463	0.487	0.482
8	0.471	0.490	0.487
9	0.481	0.492	0.489
10	0.485	0.493	0.491

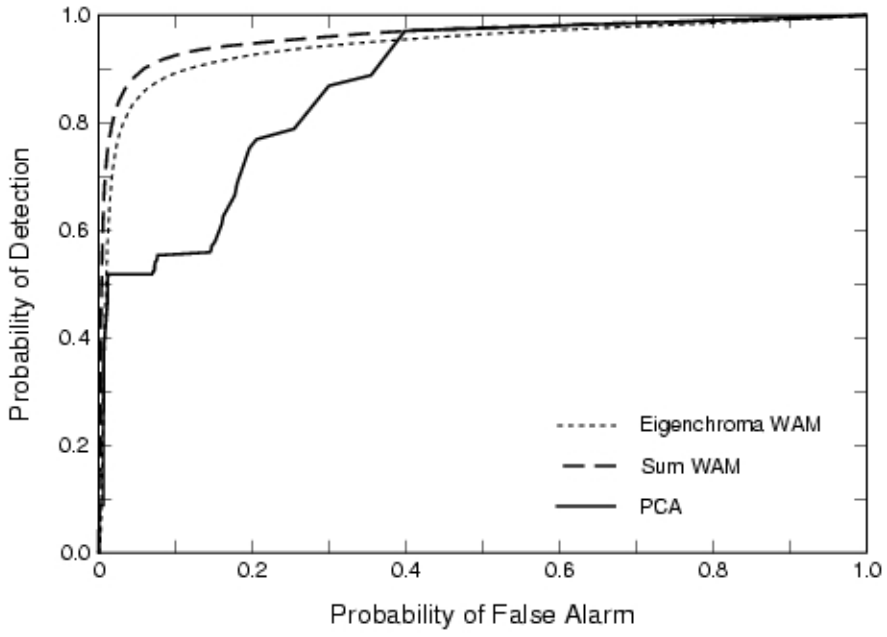

Fig. 8. ROC curves for 3% target embedded in visible data.

Our final example is in the SWIR spectral range. A representative image from the data cube is shown in Fig. 9, followed by the algorithm results in Fig. 10 for a 3% embedded target.

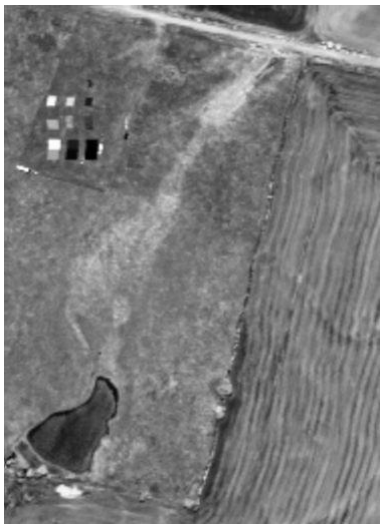

Fig. 9. Representative image from SWIR hypercube. Embedded pixel extracted from one of the panels in the upper left corner of the image.

Fig. 10a. PCA algorithm result - no target.

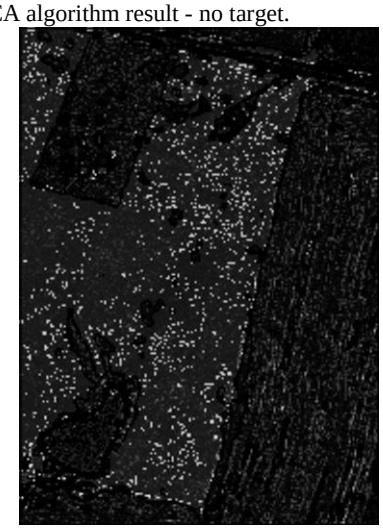

Fig. 10b. PCA algorithm result - 3% target.

Fig. 10c. PCA algorithm result - 8% target.

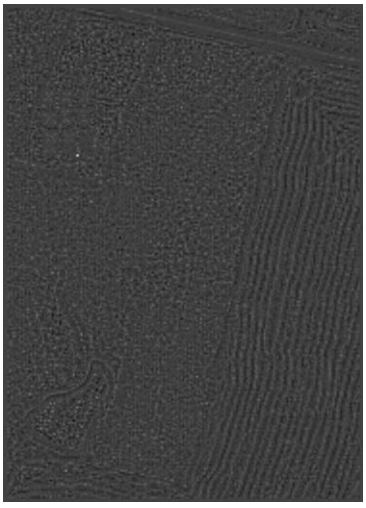

Fig. 10d. Eigenchroma – WAM algorithm result - no target.

Fig. 10e. Eigenchroma – WAM algorithm result - 3% target.

Fig. 10f. Eigenchroma – WAM algorithm result - 8% target.

Table 3 summarizes the SWIR results.

Table 3. SWIR Results.

Percent Target	PCA	Sum WAM	Eigenchroma WAM
1	0.042	0.130	0.184
2	0.141	0.236	0.303
3	0.226	0.311	0.371
4	0.280	0.363	0.413
5	0.284	0.398	0.439
6	0.313	0.423	0.456
7	0.355	0.441	0.467
8	0.386	0.454	0.474
9	0.412	0.463	0.479
10	0.427	0.470	0.482

Once again the weighted anti-median result is the best. The Eigenchroma sum is a better result than just summing the individual band results. The ROC curve for the 3% target is in Fig. 11. The shape of the ROC curve, its very slow rise to a P_D equal to one, indicates the difficulty of obtaining all of the targets. The image shown in Fig. 9 does not contain a field stop (the border around the image). Since in the previous images the field stop was a particularly easy area to detect the target, we would expect the ROC curves in Fig. 11 and the values in Table 3 to be lower.

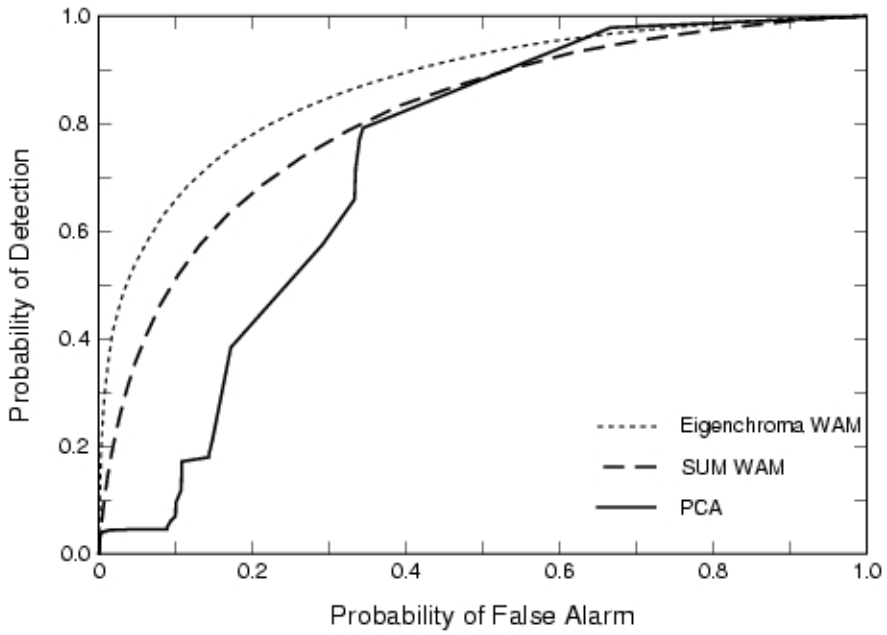

Fig. 11. ROC curves for 3 % target embedded in SWIR image.

7. CONCLUSIONS

We have presented two methods to detect point targets in hyperspectral data. Results show that relatively low percentage point targets are easily detected in three spectral regions. Our method of inserting fractional targets allows us to evaluate the algorithmic performance without relying on actual test data.

The weighted anti-median algorithm performed better in all cases tested. The superiority of the weighted anti-median algorithm over the principal component analysis algorithm was not anticipated. Our implementation gave the principal component analysis algorithm advantages over the anti-median filter. We eliminated from consideration all points that were not internal to a single cluster. Since edge points are one of the main source of clutter leakage for point target detection, we expected a superior result. Nevertheless, the anti-median method was superior in all cases. It appears that processing of each of the bands individually provides valuable information in quantifying the presence of targets. This demonstrates that hyperspectral data itself is extremely valuable; one should avoid compressing it too readily.

This work is very rich in possible future extensions. Additional research on both methods is desirable. The principal component algorithm could be improved by using different principal component images. Sophisticated methods for producing optimum (for point target extraction) principal component images should be investigated. When merited by image quality, the method could be extended by employing the statistics from three or more principal component images. The richness of the hyperspectral data cube is demonstrated very well by the results of the weighted anti-median algorithm. A simple summing gave excellent results, and weighting the bands by the first eigenchroma gave slightly better results in two out of three examples. Future work, both theoretical and experimental, is planned to optimize the weighting function of the bands, which should yield even better results.

ACKNOWLEDGMENTS

The cameras used to collect the visible and MWIR data were designed and fabricated by William Ewing, Toby Reeves and Steven DiSalvo. The HYDICE data was provided by Spectral Information Technology Application Center (SITAC). We are grateful to the following colleagues: Virgil Vickers for critical review of the manuscript and Linda Bouthillette for graphic assistance. This work was carried out under Air Force Task 2305BN00. We'd like to acknowledge partial support of the Paul Ivanier Center for Robotics and Industrial Production, Beer-Sheva, Israel. This work was performed while one of the authors (SRR) held a National Research Council Research Associateship Award at the Air Force Research Laboratory at Hanscom AFB.

REFERENCES

1. D.S.K. Chan, "A unified framework for IR target detection and tracking," in *Signal and Data Processing of Small Targets 1992*, O. E. Drummond, Editor, Proceedings of SPIE Vol. 1698, pp. 66-76, 1992.

2. J.S. Acetta, "Infrared search and track systems," Chap. 4 in Passive Electro-Optical Systems, V. 5 of the *Infrared Electro-Optical Systems Handbook*, S. B. Campana, Ed., pp. 209-344, ERIM and SPIE, Ann Arbor MI, 1993.

3. C. E. Caefer, J. Silverman, and J.M. Mooney, "Optimization of Point Target Tracking Filters", IEEE Trans. on Aerospace and Electronic Systems, 36(1), pp. 15-25, 2000.

4. M. Bar-Tal and S.R. Rotman, "Performance Measurement in Point Target Detection," Inf. Phys. Tech., 37, pp. 231-238 (1996).

5. R. Succary, A. Cohen, P. Yarctzi, S.R. Rotman and S. Nadav, "Dynamic Programming Algorithm for Point Target Detection: Practical Parameters for DPA", in *Signal and Data Processing of Small Targets 1992*, O.E. Drummond, Editor, Proceedings of SPIE Vol. 4473, pp. 96-100, 2001.

6. J. Silverman, C.E. Caefer, J.M. Mooney, M.M. Weeks, and P. Yip, "An automated clustering/segmentation of hyperspectral images based on histogram thresholding", in *Imaging Spectrometry VII*, M.R. Descour and S.S. Shen, Editors, Proceedings of SPIE Vol. 4480, pp. 65-75, 2001.

7. I. S. Reed and X. Yu, "Adaptive Multiple-Band CFAR Detection of an Optical Pattern with Unknown Spectral Distribution", IEEE Trans. on Acoustics, Speech, and Signal Processing, 38(10), pp.1760-1770, 1990.

8. D. W. Paglieroni and D.E. Perkins, “Automatic extraction of closed pixel clusters for target cueing in hyperspectral images”, in *Signal and Data Processing of Small Targets 2001*, O.E. Drummond, Editor, Proceedings of SPIE Vol. 4473, 51-61, 2001.

9. J. E. Murguia, T. D. Reeves, J. M. Mooney, W. S. Ewing, F. D. Shepherd, and A.K. Brodzik, "A compact visible/near infrared hyperspectral imager", in *Infrared Detectors and Focal Plane Arrays*, E.L. Dereniak and R.E. Sampson, Editors, Proceedings of SPIE Vol. 4028, 457-468, 2000.

10. J. M. Mooney, V. E. Vickers, M. An, and A.K. Brodzik, "High throughput hyperspectral infrared camera", *J. Opt. Soc. Am. A*, 14(11), pp. 2951-2961, 1997.

11. R. A. Schowengerdt, *Remote Sensing*, Chap. 1, Academic Press, San Diego, 1997.